MOLECULAR DYNAMICS SIMULATIONS OF VOID MORPHOLOGY IN CRYSTALLINE SILICON: TEMPERATURE DEPENDENCE

Tomohiko Ogata, Keita Ogasawara, Shinji Munetoh, Teruaki Motooka
Department of Materials Science and Engineering, Kyushu University, 744 Motooka, Fukuoka, 819-0395, Japan

Introduction

Defect-free silicon (Si) wafers are essential for microelectronics device fabrications. Microdefects, for example, cause dielectric breakdown of gate oxides in MOS devices [1,2]. These microdefects are mainly voids formed from vacancies introduced at the solid/liquid interface into crystal Si ingot during CZ and FZ processes.

Morphology of the void is determined during the cooling processes for crystallization in the CZ and FZ methods. By taking into account of the low surface energy of the Si{111} surface, the octahedral void is preferable in crystalline Si. The void obserbed on Si wafers are called as the Scattering Tomograpy Defect (LSTD) as illustrated in Fig.1(a) [3], Crystal Oriented Particle (COP) [4] and Flow Pattern Defect (FPD) [5], which are octahedral void in Si ingot before cutting the ingot. However, the observed void morphology is changed by the cooling rate and impurities. Another morphology of void is "cloud-like void" in FZ-Si wafers by high cooling rate as illustrated in Fig.1(b) [6].

Molecular dynamics (MD) simulation is the powerfull tool to analyze the atomistic dynamics at high temperatures. We have investigated melting and crystallization processes of amorphous Si (a-Si) during the excimer laser annealing by using MD simulations [7-9]. The simulated results well reproduced the observed melting rate and elucidated the mechanism of crystallization in Si thin film. Furthermore, various MD simulations have been performed in order to clarify the role of defects [10-12].

In this paper, we performed MD simulations in order to investigate the stable void morphologies at various temperatures below the melting point of Si. We also discuss the transitions between these morphologies at various cooling rates.

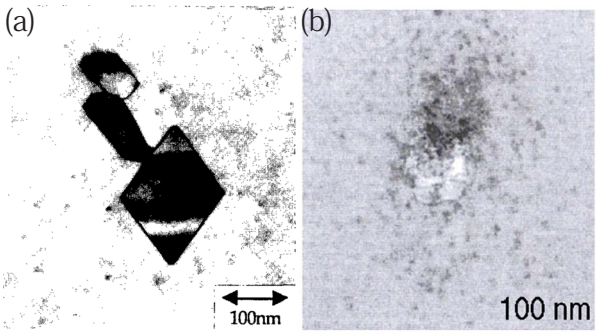

Fig. 1. Void morphorogies observed in CZ and FZ Si crystals at various conditions: (a) Triple octahedral void called LSTD, (b) primari void and surrounding small voids called by cloud-like void. Taken from Refs 3 and 6.

Calculation method

MD simulations were performed by using Tersoff potential [13-15]. Although by using Tersoff potential the melting point (T_m) of crystalline Si is approximately 2580K, different to the experimental value of 1685K, the structures of liquid Si (l-Si) or a-Si can be well reproduced with this potential [16,17]. Periodic boundary conditions were used in each direction. Temperature was controlled by using Langevin equation. The time step was set at 2fs and the friction coefficient was chosen to be $5ps^{-1}$.

The initial configuration is crystalline silicon with octahedral void prepared by removing atoms in a MD cell. Figure 2(a) is initial configuration of silicon atoms in a MD cell with a size of $54\times54\times54Å^3$. The number of removed atoms is 84.

The observing void morphology is difficult because the void is the space between atoms. Therefore the group of vacancies which was visuallized in the space between atoms was adopted. The Si atom was inserted into the calculation cell. The potential energy difference was calculated between the whole calculation cell with inserted Si atom and that without inserted Si atom. If the potential energy difference was less than 0.2eV, the Si atom was visuallized

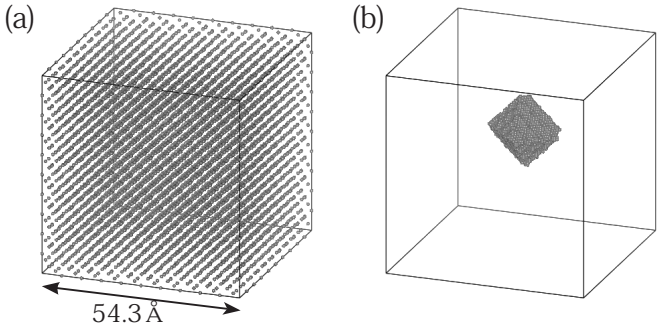

Fig. 2. Initial configurations of calculation cell.
(a) The configuration of silicon atom, which is crystalline silicon with octahedral void. (b) Visuallized void by virtual atoms.

as a vacancy. The potential energy with a inserted Si atom every 0.5Å at each directions was repeatedly calculated in order to scan the vacancies. The group of vacancies was regarded as a void. Figure 2(b) shows the void morphology visuallized from Fig.2(a).

Results and Discussion

Figure 3 shows the snapshot of the morphology of void during annealing at 2450K from initial condition. The void morphology is aggregated configuration like a octahedral.

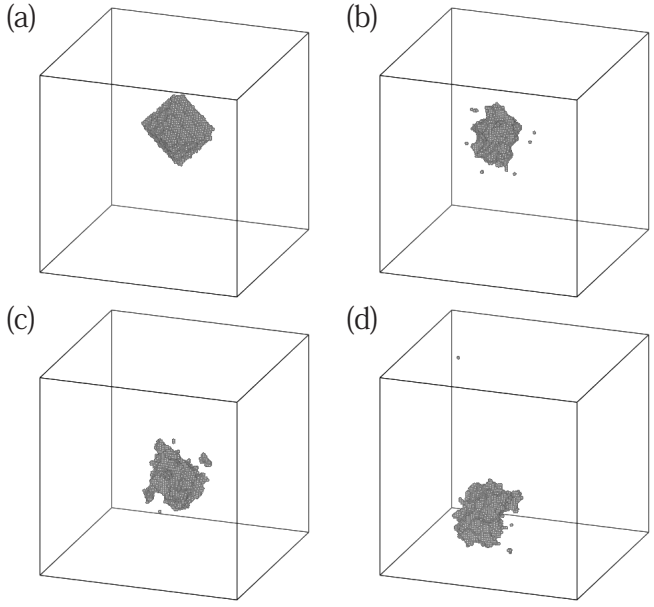

Fig. 3. Snapshots of void morphorogies during annealing at 2450K in calculation cell with 84 removed atoms: (a) initial, after (b) 1ns, (c) 10ns and (d) 20ns.

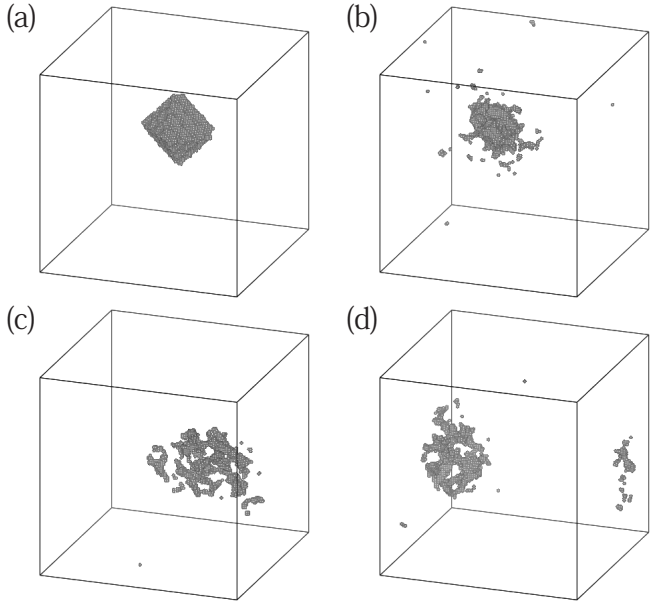

Fig. 4. Snapshots of void morphorogies during annealing at 2550K in calculation cell with 84 removed atoms: (a) initial, after (b) 1ns, (c) 10ns and (d) 20ns.

This configuration unchanged for 20ns calculation. On the other hand, at 2550K the void morphology was scattered configuration as illustrated in Fig.4. The octahedral morphology was broken around 2ns. After transformation to the scattered void as illustrated in Fig.4(c), the void morphology was not changed from 20ns.

Figure 5(a)-(d) show the snapshots of the morphology of void and Fig.5(e) shows the potential energy during annealing at 2500K from the initial condition. At 4ns the void configuration was aggregated although the octahedral configuration was breaked as illustrated in Fig.5(b). At 10ns the configuration of void change from aggregated configuration to scattering configuration of small voids as illustrated in Fig.5(c). The potential energy increased

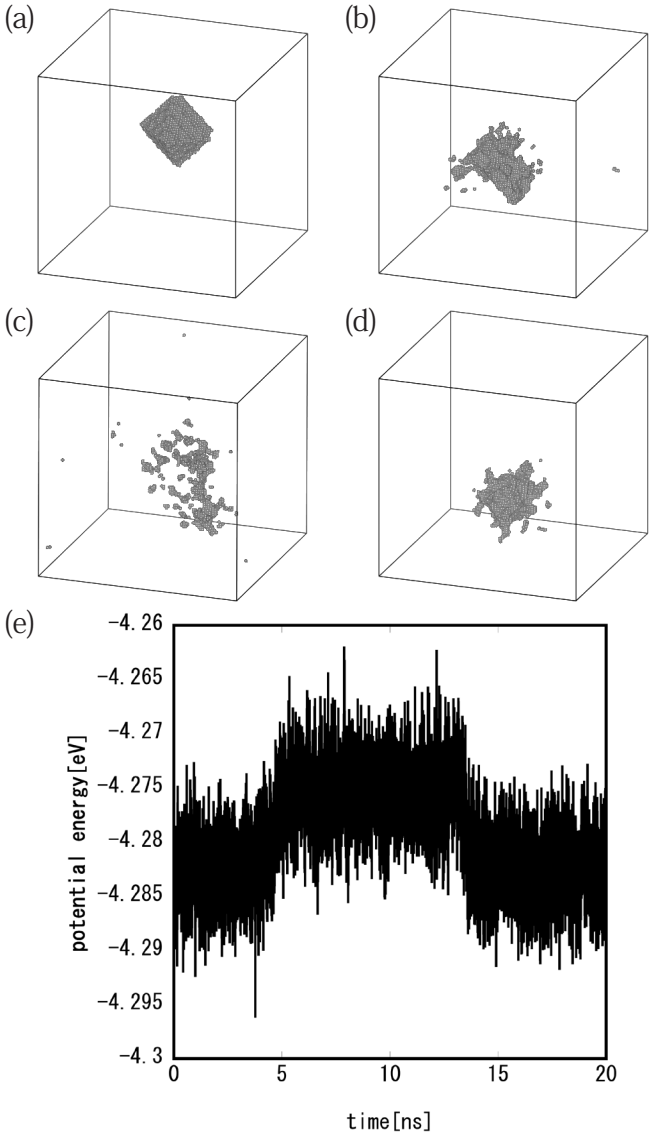

Fig. 5. Snapshots of void morphorogies and potential energy during annealing at 2500K in calculation cell with 84 removed atoms: (a) initial, after (b) 4ns, (c) 10ns and (d) 16ns. (e) potential energy as a function of time on this condition.

between 4ns and 10ns in Fig.5(e). At 16ns the scattered small voids were aggregated again as illustrated in Fig.5(d). The potential energy dropped between 10ns and 16ns. The transition of configuration occurred repeatedly for 60ns. At 2450K the void configuration was aggregated and at 2550K the void configuration was scattered small voids for 20ns. The transition temperature between aggregated and scattered morphology is around 2500K in the crystalline silicon with 84 removed atoms.

We can explain this transition by means of the free energy of the aggregated configuration and the scattered configuration. At 2450K the free energy of the aggregated void is lower than that of the scattered void. On the other hand, at 2550K the free energy of the scattered void is lower than that of aggregated void. Between 2450K and 2550K, the free energy of the scattered and the aggregated void are the same. The equal free energy of the calculation cells of two morphologies cause transformation of two morphologies around 2500K.

Figure 6 is the transition temperature of void morphology as a function of the number of removed atoms from the perfect crystalline silicon with a size of $54\times54\times54\text{Å}^3$. The morphology of void at higher temperature than critical temperature was scattered while the morphology of void is aggregated at lower temperature than that. The transition temperature increases with increasing the number of removed atoms. The critical temperature approach the melting point of Si gradually with increasing removed atom.

We performed the calculation of cooling condition from

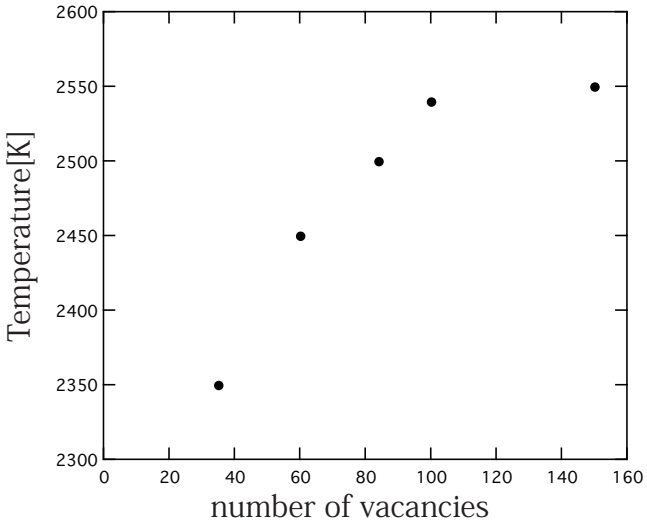

Fig. 6. The critical temperature in which the void morphology transit from aggregated configuration to scattered configuration. The number of vacancies means the number of removed atoms from crystalline Si in initial calculation cell.

the scattered small voids configuration in order to reproduce high cooling rate. The initial configuration was produced by annealing for 8ns at 2500K from the crystalline silicon with octahedral void. Figure 7 shows the morphology of void during cooling the whole MD cell on condition that the cooling rate is $1.0\text{x}10^{11}$ K/s. The voids were aggregated and made a large void. Figure 8 shows the morphology of void during cooling the whole MD cell on condition that the cooling rate is $4.35\text{x}10^{11}$ K/s. On this condition large core void and small voids around the core was produced by the aggregation of small voids. After the cooling under 1600K

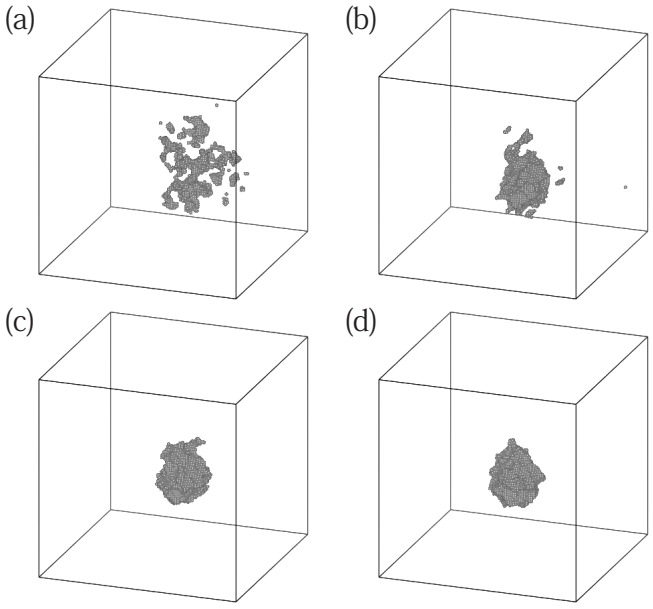

Fig. 7. Snapshots of void morphorogies on condition that the cooling rate $1\text{x}10^{11}$ K/s. (a) initial morphology, after (b)3.5ns, (c)5.0ns and (d)8.5ns.

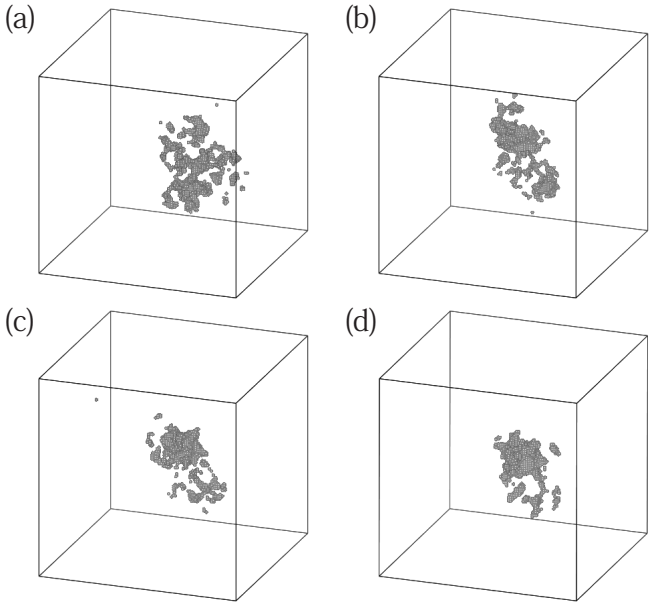

Fig. 8. Snapshots of void morphorogies on condition that the cooling rate $4.35\text{x}10^{11}$ K/s. (a) initial morphology, after (b)0.8ns, (c)1.2ns and (d)2.0ns.

after 2.0ns, the voids hardly diffused because temperature is low. Figure 1(b) shows "cloud-like void" ,which is primary void surrounded by secondary small voids cluster cloud in FZ crystal with very high cooling rate. In our simulations, the morphology of void is cloud-like at high cooling rate ($4.35x10^{11}$ K/s) although the morphology of void is one sphere at low cooling rate($1.00x10^{11}$ K/s). We indicate that the high cooling rate is one of factor of cloud-like void in FZ silicon.

Conclusion

The dependence of the morphology of voids in silicon crystal is investigated. The aggregated morphology was observed at 2450K in the calculation cell of crystalline silicon with 84 removed atoms. On the other hand, The scattered morphology was observed at 2550K in the same calculation cell. The critical temperature between the aggregated morphology of void and the scattered morphology of void exists under the melting point. This phenomenon is the same of the free energy between aggregated morphology and scattered morphology at the critical temperature. The critical temperature is the function of number of vacancy. The void morphology change primary void and secondary small voids like a "cloud-like void" in FZ-Si due to high cooling rate.

References

1. Park, J. G. and Rozgonyi, G. A. DRAM Wafer Qualification Issues: Oxide Integrity vs. D-Defects, Oxygen Precipitates and High Temperature Annealing. *Solid Stat. Phenom.,* **47-48**(1996) 327-352.
2. Furuya, H., Nakajima, K., Furukawa, J. and Shingyouji, T. Defect Recognition and Image Processing in Semiconductors and Devices Conf. *Inst. Phys. Conf. Ser.,* **135**(1993) 11.
3. Sadamitsu, S., Umeno, S., Koike, Y., Hourai, M., Sumita, S. and Shigematsu, T. Dependence of the Grown-in Defect Distribution on Growth Rates in Czochralski Silicon. *Jpn. J. Appl. Phys.,* **32**(1993) 3675-3681.
4. Ryuta, J., Morita, E., Tanaka, T. and Shimanuki, Y. Crystal-Originated Singularities on Si Wafer Surface after SC1 Cleaning. *Jpn. J. Appl. Phys.*, **29**(1990) L1947-L1949.
5. Yamagishi, H., Fusegawa, I., Fujimaki, N. and Katayama, M. Recognition of D defects in silicon single crystals by preferential etching and effect on gate oxide integrity. *Semicond. Sci. Technol.*, **7**(1992) A135-A140.
6. Vanhellemont, J., Dornberger, E., Esfandyari, J., Kissinger, G., Trauwaert, M. A., Bender, H., Graf, D., Lambert, U., Ammon, W. V. Mater. *Sci. Forum, ICDS*, **19** (1997).
7. Ogata, T., Mitani, T., Munetoh, S. and Motooka, T. Crystallization Processes of Amorphous Si During Excimer Laser Annealing in Complete-melting and Near-complete-Melting Conditions: A Molecular Dynamics Study. *Mater. Res. Soc. Symp. Proc.*, **1150E**(2008) RR04-07.
8. Motooka, T., Munetoh, S., Kishikawa, R., Mitani, T. and Ogata, T. Controlling the Nucleation Site and Crystal Orientation during Eximer-laser Annealing Processes in Thin Amorphous Si Films on Glass: A Molecular-dynamics Study. *ECS Transactions*, **8**(2007) 191-196.
9. Motooka, T., Munetoh, S., Kishikawa, R., Kuranaga, T., Ogata, T. and Mitani, T. Molecular-Dynamics Simulations of Recrystallization Processes in Silicon: Nucleation and Crystal Growth in the Solid-Phase and Melt. *ECS Transactions*, **3**(2006) 207-213.
10. Ishimaru, M., Munetoh, S., Motooka, T., Moriguchi, K. and Shintani, A. Molecular-dynamics studies on defect-formation processes during crystal growth of silicon from melt. *Phys. Rev B*, **58**(1998) 12583-12586.
11. Nishihira, K. and Motooka, T. Molecular dynamics simulations of crystal growth from melted Si: Self-interstitial formation and migration. *Phys. Rev. B,* **66**(2002) 233310-1-233310-4.
12. Motooka, T., Nishihira, K., Oshima, R., Nishizawa, H. and Hori, F. Atomic Diffusion at Solid/Liquid Interface of Silicon: Transition Layer and Defect Formation. *Phys. Rev. B*, **65**(2002) 081304-081307.
13. Tersoff, J. Modeling solid-state chemistry: Interatomic potentials for multicomponent systems. *Phys. Rev. B,* **39**(1989) 5566-5568.
14. Tersoff, J. Carbon defects and defect reactions in silicon. *Phys. Rev. Lett.*, **64**(1990) 1757-1760.
15. Tersoff, J. Chemical order in amorphous silicon carbide. *Phys. Rev. B*, **49**(1994) 16349-16352.
16. Ishimaru, M., Yoshida, K. and Motooka, T. Application of empirical interatomic potentials to liquid Si. *Phys. Rev. B*, **53**(1996) 7176-7181.
17. Ishimaru, M., Munetoh, S. and Motooka, T. Generation of amorphous silicon structures by rapid quenching: A molecular-dynamics study. *Phys. Rev. B,* **56**(1997) 15133-15138.